Desalination and Water Treatment
www.deswater.com
doi: 10.5004/dwt.2022.28267

252 (2022) 339–347
March

Photocatalytic degradation of water disinfection by-products using zirconium doped zinc oxide nanoparticles

Soudabeh Dadvar[a], B. Shahmoradi[a,*], Shaho Habibi[b], K. Wantala[c], Totsaporn Suwannaruang[c], Afshin Maleki[d], H.P. Shivaraju[e], Seung-Mok Lee[f,*]

[a]*Department of Environmental Health, Faculty of Health, Kurdistan University of Medical Sciences, Sanandaj, Iran, emails: bshahmorady@gmail.com (B. Shahmoradi), sdadvar97@yahoo.com (S. Dadvar), maleki43@yahoo.com (A. Maleki)*
[b]*Department of Water Quality Control, Kurdistan Water and Wastewater Company, Sanandaj, Iran, email: sh.habibi1399@gmail.com (S. Habibi)*
[c]*Department of Chemical Engineering, Faculty of Engineering, Khon Kaen University, Thailand, emails: kitirote@kku.ac.th (K. Wantala), totsaporn.eng.kku@gmail.com/totsaporn.s@kkumail.com (T. Suwannaruang)*
[d]*Department of Environmental Health, Environmental Health Research Center, Research Institute for Health Development, Kurdistan University of Medical Sciences, Sanandaj, Iran, email: maleki43@yahoo.com (A. Maleki)*
[e]*Department of Water & Health-Faculty of Natural Sciences, JSS Academy of Higher Education & Research, Sri Shivarathreeshwara Nagara, Mysuru-570015, Karnataka, India, email: shivarajuenvi@gmail.com/shivarajuhp@jssuni.edu.in (H.P. Shivaraju)*
[f]*Department of Environmental Engineering, Catholic Kwandong University, Gangneung 25601, Korea, email: leesm@cku.ac.kr (S.-M. Lee)*

Received 5 November 2021; Accepted 3 February 2022

ABSTRACT

The aim of this study was to investigate the photocatalytic decomposition of disinfection by-products using zinc oxide nanoparticles doped with zirconium (Zr:ZnO NPs). Zr:ZnO NPs were synthesized through mild hydrothermal method. The characterization of Zr:ZnO NPs was performed using X-ray diffraction, SEM, Fourier-transform infrared spectroscopy, dynamic light scattering, and zeta potential. Photodegradation of trihalomethanes was investigated as a disinfection by-product of chlorinated water under sunlight and UV light illumination. The optimum conditions for removal of trihalomethanes under UV irradiation was 2 h contact time, 1% Zr:ZnO NPs and nanoparticles dosage of 1.5 g/L so that the removal percentages for bromoform, bromomethane chloride, dichlorobromomethane, and total trihalomethane were 79.25%, 96.5%, 65% and 52%, respectively. No chloroform was degraded under this condition. The optimum conditions under sunlight illumination occurred at 2 h contact time, 1.5% Zr:ZnO NPs and nanoparticles dosage of 2.0 g/L occurred so that the removal percentages for chloroform, bromoform, bromomethane chloride, dichlorobromomethane, and total trihalomethane were 20%, 88.5%, 99.75%, 65%, and 67%, respectively. Investigation of the photocatalytic properties of the samples showed the positive presence of a metal as dopant to improve the photocatalytic properties of the samples, so that Zr:ZnO showed 42% higher efficiency compared with bare ZnO in photocatalytic decomposition of trihalomethanes.

Keywords: Zr:ZnO nanoparticles; Photocatalyst; Disinfection by-products; Hydrothermal; Characterization

1. Introduction

Water is one of the basic human needs. Water pollution is a growing issue nowadays. The problem has become more acute and complicated due to the entry of various pollutants and the pollution of existing water resources and the decline of water quality. Today, these water sources are usually exposed to various pollutants [1]. The most important

* Corresponding authors.

pollutants are turbidity, natural organic compounds (NOM), different types of insecticides used in agriculture, and chemical compounds excreted by effluents of various industries [2]. Water treatment plants apply different chemicals and technologies developed to make water safe for drinking. Due to lots of technical, cultural, and operational issues, the most common method of drinking water disinfection in developing countries is chlorination [3]. Although the use of chlorine as an oxidizer and destroyer of microorganisms has many advantages, but its use also has certain disadvantages. It has one of the most important chlorine disinfectants (DBPs) such as trihalomethanes (THMs) and halostatic acids (HAAs), generated due to the combination and reaction of chlorine and its compounds with surface and groundwater precursors, that is, NOM [4].

The World Health Organization (WHO) reports that THMs have the highest concentrations of DBPs [5]. The EPA has also reported that THMs include four groups of compounds, including chloroform, bromodichloromethane, dibromochloromethane, and bromoform [6]. The formation of THMs depends on many factors such as pH, chlorine contact time, chlorine concentration and properties, residual chlorine, temperature, amount of NOM and bromine concentration [7]. Increasing the pH and contact time increases the production of trihalomethanes [8].

There are several methods for removing disinfection by-products, including adsorption, activated carbon [9], ion exchange [10], coagulation and flocculation by polymeric materials [11], alum [12], iron and sulfate [13], membrane processes [14] and photocatalytic processes [15].

The photocatalytic method is a subset of advanced oxidation processes (AOPs) in which organic or toxic contaminants are eliminated by light degradation. The use of photocatalytic methods has advantages over other methods of treatment of organic pollutants, including the complete destruction of chemicals and their conversion into low-harmful chemicals, degradation of highly stable compounds, very good performance at ambient temperature and pressure, no need to inject oxygen, no pollution in the final product, as well as economics and advanced technology [16,17].

Among the photocatalytic materials used to eliminate organic and inorganic contaminants are TiO_2, MoS_2, WO_3, Fe_2O_3, ZnO and CdS [18]. ZnO has been considered by researchers due to its high volume to surface ratio as well as optical, photochemical, catalytic properties, long service life and more reasonable cost-effectiveness [19]. In the advanced oxidation process, the compounds can be completely mineralized and converted to carbon dioxide and water by the hydroxyl radical, which is a strong oxidizing agent [20].

One of the excellent methods for synthesizing doped ZnO nanoparticles is mild hydrothermal technique [21]. In general, metal nanoparticles in aqueous solutions tend to accumulate and form agglomeration, so they may be hydrophobic. In the case of nanoparticles, various surface modifications were performed on them to prevent agglomeration. These techniques prevent nanoparticles from clumping. In this method, by adding surfactant, not only agglomeration but also surface oxidation can be prevented [22].

One of the goals in improving the performance of nanocatalysts is to shift the response range of UV wavelengths to the visible light region. There are several ways to achieve this goal. One of these methods is doping nanostructures with other elements, which changes the electronic properties of the nanocatalyst and ultimately changes its optical response through changing band gap energy [23]. Doping has been considered as an effective method to improve and enhance the properties and characteristics of ZnO for various applications [24]. Suitable doping can result in activating ZnO under visible light as a driven energy [25,26].

Many intermediate metals including Fe, Co, Ni, Mn, Cu and Zr are used as dopant [27,28]. Doped photocatalyst activity is a function of doping percentage and doping energy levels, electronic configuration, doping distribution, electron concentrating and light intensity [29,30]. Zirconium is a non-toxic, low cast material with a band gap energy of 5 eV, such properties would make it a suitable element to be considered as dopant for ZnO [31]. Therefore, it can reduce the band gap energy of ZnO, so that the final product could be active under sunlight illumination. Thus, the aim of this study was to determine the photocatalytic decomposition of disinfection by-products using zinc oxide nanoparticles doped with zirconium (Zr:ZnO NPs) under different light sources and intensities.

2. Materials and methods

2.1. Synthesis of Zr:ZnO NPs

Synthesis of Zr:ZnO NPs was performed under mild hydrothermal conditions. In brief, 1 g of 2 M zinc nitrate (Merck, Germany) was poured in a Teflon liner and zirconium acetate (Sigma-Aldrich, USA) with different weight percentages (0.5%, 1.0%, and 1.5%) was added as the dopant precursor. Then 10 mL of 1 M sodium hydroxide (Merck, Germany) as a solvent and1 mL of n-butylamine, as surface modifier, was added to it and mixed gently for a few minutes using a glass rod to obtain a homogeneous mixture. Finally, the Teflon liner was sealed and placed in a General-Purpose autoclave. The assembled was kept in an oven at 120°C for 12 h. After the reaction time, the Teflon liner was removed from the autoclave and its content was poured into a falcon tube by adding distilled water; it was centrifuged at 4,000 rpm until the pH became neutral. Then the product was dried at room temperature (40°C). The final nanoparticles fabricated were kept in desiccator until characterization and systematic photodegradation studies.

2.2. Characterization of Zr:ZnO NPs

The instruments used for characterization of Zr:ZnO NPs X-ray diffraction (XRD) analysis (PANalytical, Model X'Pert PROMPD; Netherland). Field-emission scanning electron microscopy (FE-SEM) images (Model FE-SEM SU-70, Hitachi, Japan), Fourier-transform infrared (FTIR) spectrophotometer (Model ALPHA, USA), X-ray photoelectron spectroscopy (XPS), dynamic light scattering (DLS) (DLS Omni model made by Brook Haven, USA) and zeta potential (DLS Omni made by Brook Haven, USA).

2.3. Photodegradation experiments

The photodegradation efficacy of the nanoparticles synthesized was investigated using a solution of

trihalomethanes. Stoke solution was initially made from trihalomethane compounds. Due to the fact that these trihalomethanes include four substances, chloroform, bromoform, dibromomethane and dichloromethane, to prepare a solution of 1,000 ppm as a stock solution, the density of each material was considered and a solution of 1,000 ppm of each analyte was made. For example, considering that the density of chloroform (ρ = 1.48 g/mL), a value of 0.67 mL of chloroform, 0.34 mL of bromoform, 0.4 mL of dibermomethane, and 0.75 mL of dichloromethane was taken and poured into a 1000 mL conical flask and made to volume using distilled water. Operating concentrations were then prepared from the stock solution to which a certain amount of synthesized nanoparticles was added to the trihalomethane solution, and after a certain period of time intervals, the efficiency of the nanoparticles was investigated. Before photodegradation studies under light illumination, each sample was kept in darkness for 1 h under continuous shaking (ω = 100 rpm) to ensure adsorption–desorption equilibrium. At each step, by changing one parameter and keeping the other parameters constant, the removal efficiency of trihalomethanes using Zr:ZnO NPs, the effect of existing parameters was investigated. The studied parameters were the dosage of Zr:ZnO NPs (0.5, 1, 1.5, and 2 g/L), contact time (30, 60, 90, and 120 min), and light source (UV and sunlight) at fixed concentration of trihalomethane (40 ppb); this concentration was the maximum concentration level of trihalomethane reported in the study area. In order to check adsorption/desorption equilibrium, a sample containing 40 ppb trihalomethanes and Zr:ZnO NPs was kept in darkness over a shaker (ω = 120 rpm) for 1 hr. Then, by concentrating the specified light source, each sample was exposed to sunlight and UV lamp (2 lamps 15 W, 45 cm UV lamps made by Philips Netherlands), separately. The samples were exposed to sunlight at 12:00 to 14:00, when the intensity of the sunlight was the highest and were sampled at different time intervals. The UV intensity was measured using UVA meter (CHY, Taiwan) and sunlight intensity was measured using LUX meter (Lutron, Taiwan). The mean intensity of sunlight and ultraviolet intensity were +20000 LUX and 1.5 w/m^2, respectively. Finally, the concentration of the trihalomethane was recorded following the EPA method study 23B, Method 501.2, trihalomethanes by Liquid/Liquid extraction [32].

3. Results and discussion

3.1. Characterization results of Zr:ZnO NPs

FE-SEM images of Zr:ZnO NPs are shown in Fig. 1. It was found applying n-butylamine as surface modifier could control crystal growth as well as particle size. The modifier can also not only affect the dispersion of Zr:ZnO NPs, but can also change the shape and size of their particles [33]. However, the morphology of the particles was independent from the dopant weight percentage. The resulting morphology is well suited for photodegradation purposes because Zr:ZnO nanoparticles are small and well dispersed in the medium applied for photodegradation [30].

The XRD patterns show that the crystalline phase is hexagonal (Wurtzite) and has no impurities. The sharp peaks

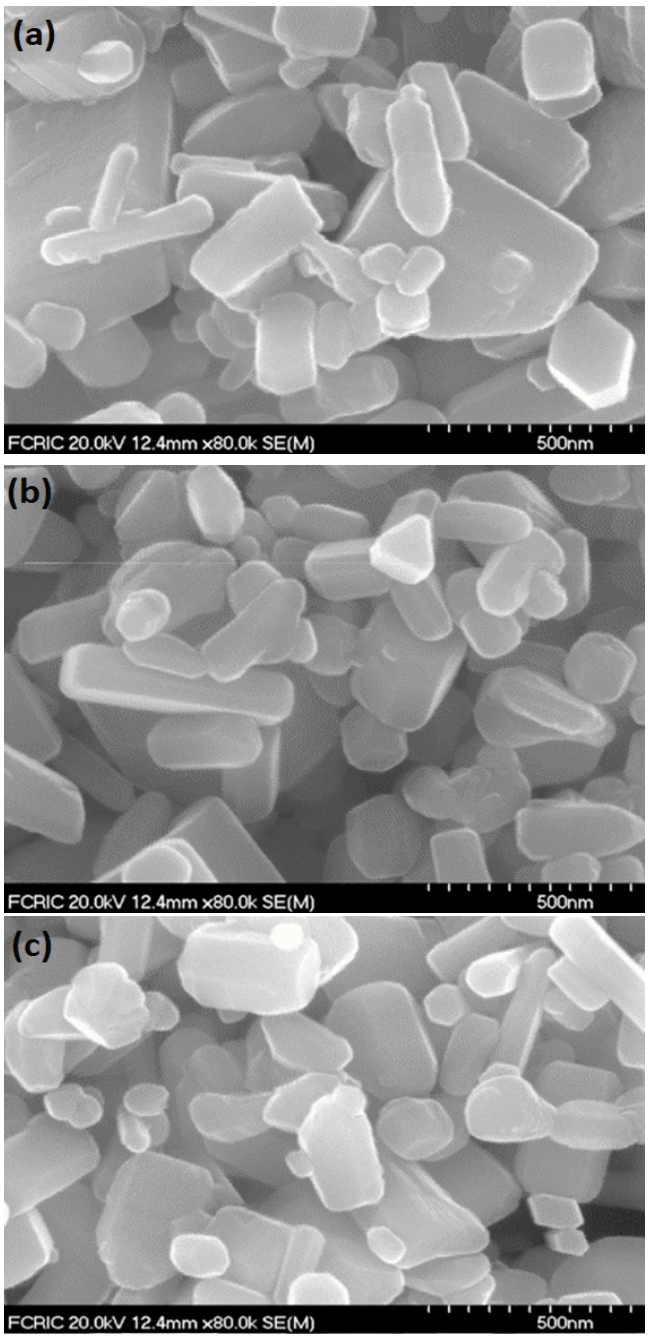

Fig. 1. FE-SEM image of Zr:ZnO nanoparticles with different percentages of dopant: (a) 0.5%, (b) 1.0%, and (c) 1.5%.

indicate good crystallization of Zr:ZnO NPs matches well with JCPDS No. 00-036-1451 of ZnO (Fig. 2). Doping ZnO with Zr did not lead to the formation of additional peaks as well as other reaction phases in the structure of ZnO lattice, which indicates that Zr is substituted in the hexagonal lattice structure. Due to the fact that zirconium has a larger ionic radius (0.82 Å) than Zn (0.74 Å), doping usually increases the lattice parameters and thus the atomic volume of the nanoparticle. X-ray diffraction results for three types of nanoparticles (different weight percentages)

showed that the crystal properties of these nanoparticles are preserved and zirconium is well doped in ZnO [34,35].

X-ray photoelectron (XPS) spectroscopy is usually performed to investigate the electron energy of the emitted photoelectrons in order to study the atomic core levels and subsequently to study the atomic compositions and their valence states in the sample [36]. Because each element possesses specific binding energy for each atomic orbital, each of these elements gives rise to a particular set of peaks. Therefore, the presence of peaks indicates the presence of a specific element in the study sample. In this result, the peaks of Zn 2p, Zr 3d, O 1s and C 1s were observed in wide-scale XPS spectra of 1.0% Zr:ZnO NPs, as shown in Fig. 3a. In addition, the contaminated C level (284.6 eV) was used to

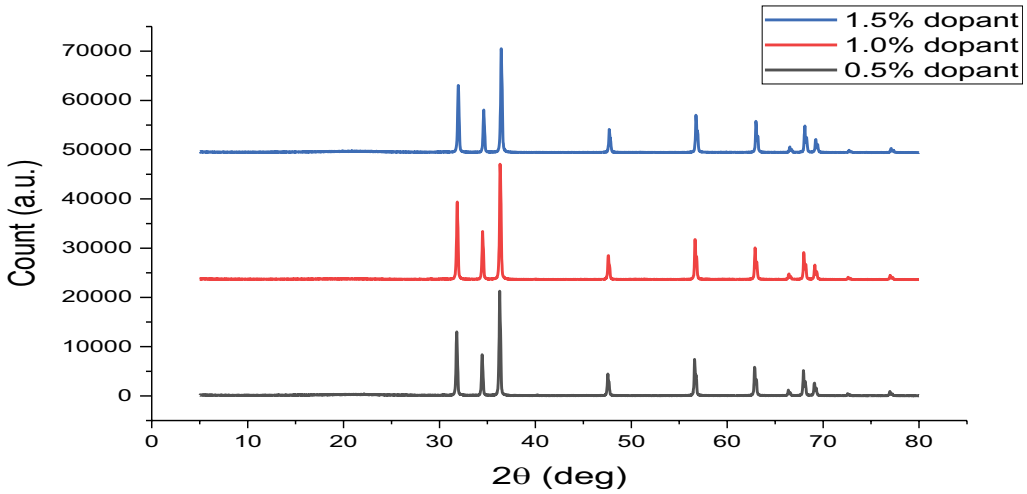

Fig. 2. X-ray diffraction patterns of Zr:ZnO nanoparticles with different percentages of dopant: (a) 0.5%, (b) 1.0%, and (c) 1.5%.

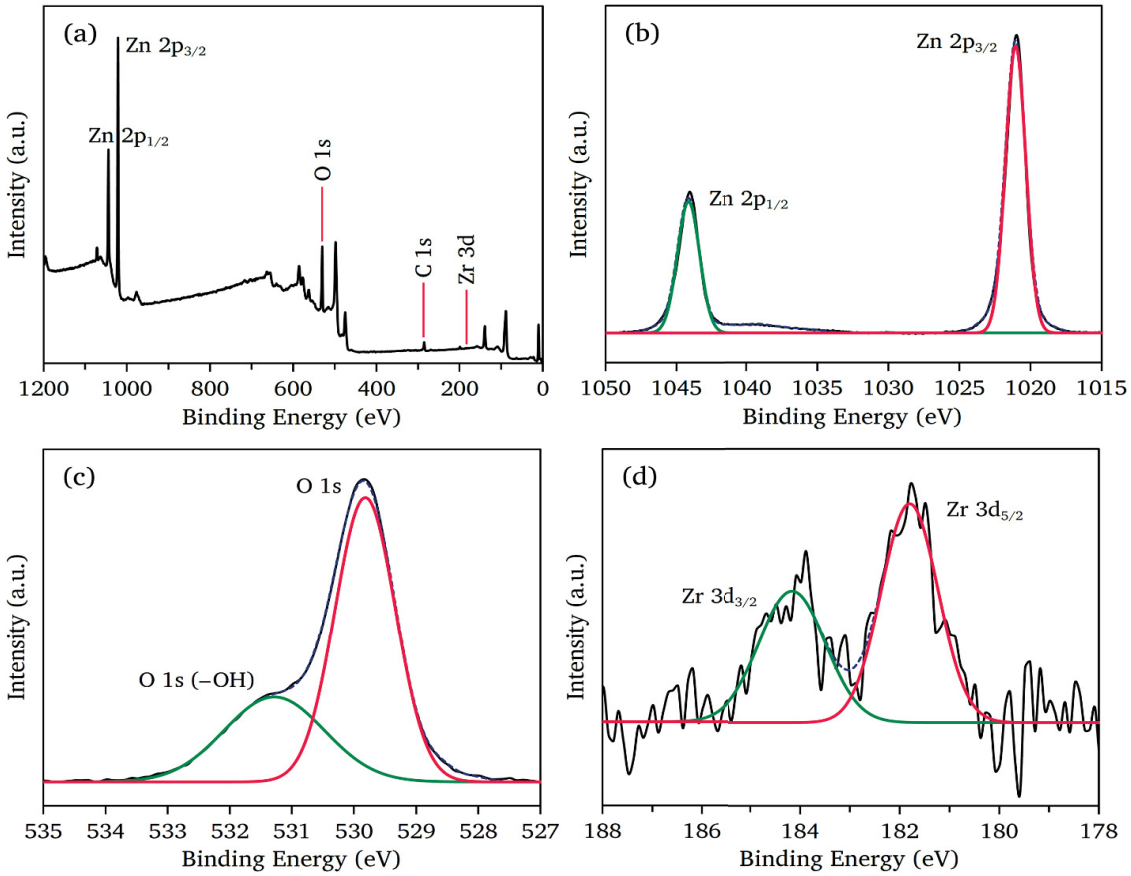

Fig. 3. Wide-survey XPS spectra (a), the high-resolution XPS scan Zn 2p (b), O 1s (c) and Zr 3d (d) of 1.0% Zr:ZnO nanoparticles.

standardize the electron binding energies of all elements. In this sample (1.0% Zr:ZnO NPs), the concentration of Zn showed the highest amount, whereas the Zr bond energy demonstrated the lowest content. As known, the peak intensities were related to the concentration of the element within the surface of the sample. Fig. 3b displays the binding energies of 1,021.0 and 1,044.0 eV, demonstrating Zn $2p_{3/2}$ and Zn $2p_{1/2}$ with Zn^{2+} in the ZnO lattice [36]. At the same time, Fig. 3c) shows the O 1s XPS spectrum of Zr:ZnO NPs. The O 1s spectra can be separated into two peaks as follows. The first peak at 529.8 eV was referred to O^{2-} in the ZnO lattice, while the second peak at 530.8 eV can be assigned to –OH group owing to chemisorption of H_2O [37]. Fig. 3d depicts the binding energies at 181.8 and 184.2 eV, representing Zr $3d_{5/2}$ and Zr $3d_{3/2}$ with Zr^{4+}, which corresponded to Zr-O bonds in the ZrO_2 [38,39]. Thus, the obtained result can be implied that the Zr atom might not substitute Zn atom in ZnO lattices, only incorporated with the interstitial site.

The FTIR spectra of Zr:ZnO NPs are shown in Fig. 4. The peak in the 450 cm^{-1} is related to Zr–O–Zr, which has also increased slightly with the increase in the amount of dopant. The peak of 620 cm^{-1} is related to Zr–OH and the bending vibration of O–Zn–O [40]. The peak in the 870 cm^{-1} is related to O–Zr–O, which has also changed slightly with the increase of dopant. The peak in 1,383 cm^{-1} is related to the Zn–O vibration [41]. The peak in 1,617 cm^{-1} is related to the tensile vibration of the OH group, which is physically adsorbed. The available peaks of 3,500–3,400 cm^{-1} are related to OH–Zn–OH vibration [31]. Moreover, the presence of n-butylamine surfactant has caused peaks in the area of 630, 870, and 1,380 cm^{-1} [42].

Size distribution of the nanoparticles synthesized was determined using DLS. As can be seen from Fig. 5, the distribution curve is skewed to the right, which has occurred due to the great abundance of fine particles compared to larger particles. According to Fig. 5, the particle size was between 1–600 nm, while higher portion had size of 50 nm, which could indicate the appropriate amount of surfactant added to the nanoparticles and the formation of smaller particles. The addition of surfactant prevents the growth of particles and ultimately better stability and prevents agglomeration and the formation of larger particles [43,44].

3.2. Photodegradation of disinfection by-products using Zr:ZnO NPs

3.2.1. Effect of dopant weight percentage

In order to determine the effect of dopant weight percentage on the photodegradation efficiency, samples with 40 ppb THMs concentration, nanoparticle dosage of 1.0 g/L, dopant percentages (0, 0.5, 1.0 and 1.5) and contact time of 120 min were exposed to UV light with 30 W intensity and sunlight illumination. In the reactor under UV irradiation, optimal removal achieved using 1.0% Zr:ZnO NPs whereas, under sunlight illumination, it was achieved using 1.5% Zr:ZnO NPs. It was found that the removal percentage increases with increasing dopant percentage because doping causes lattice defects and defects prevent electron-hole pair recombination and ultimately increased photocatalytic activity and the removal efficiency increases due to the reduction of the nanoparticle size, the effective separation of the electrons of the holes and the reduction of their recombination in the charge transfer path (Fig. 6). In UV samples, increasing the percentage of dopant to an optimal value can increase the efficiency, and when the percentage of dopant exceeds the optimal value, the presence of dopant in the particle surface prevents the adsorption of the reactant on the activated centers and the electron on the other hand. The cavities produced are unstable and may return to their stable state quickly, reducing photocatalytic activity and reducing removal efficiency [45,46].

3.2.2. Effect of contact time

To determine the effect of contact time on the photodegradation efficiency, samples with a concentration of 40 ppb from trihalomethanes were prepared by adding 1.0 g/L of 1.0 wt.% Zr:ZnO NPs and then each sample was exposed to light illumination for different time intervals (30, 60, 90 and 120 min). After the desired time, the removal efficiency

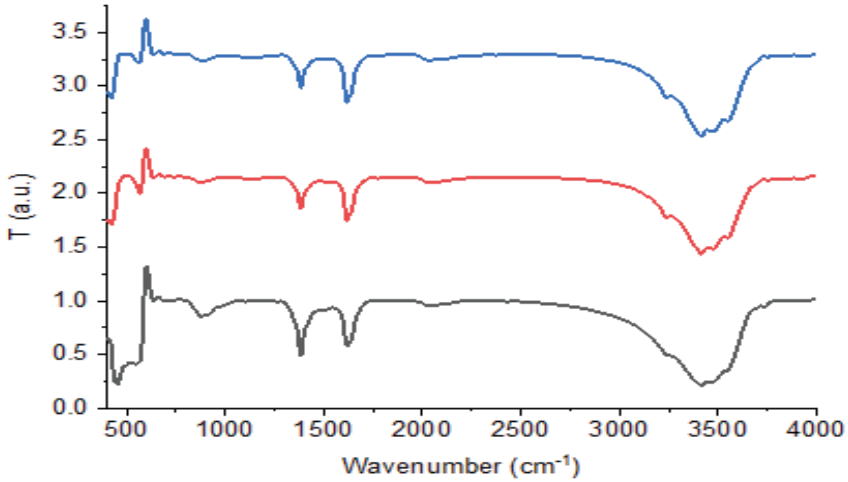

Fig. 4. FTIR spectra of Zr:ZnO nanoparticles with different percentages of dopant: (a) 0.5%, (b) 1.0%, and (c) 1.5%.

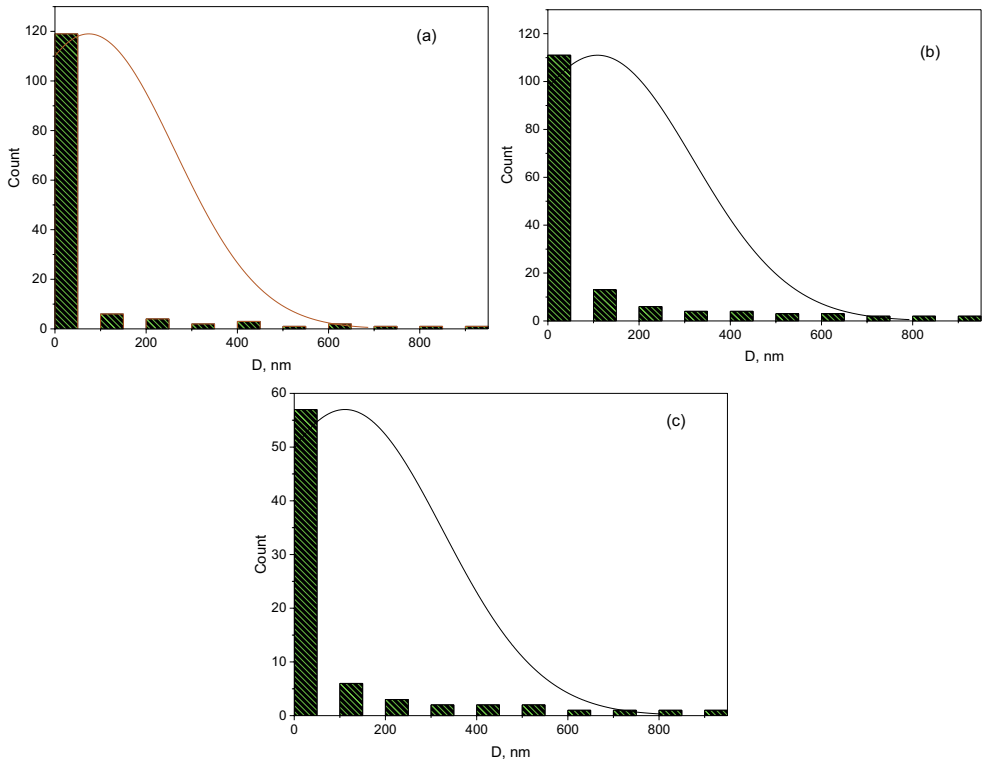

Fig. 5. DLS of Zr:ZnO nanoparticles with different percentages of dopant: (a) 0.5%, (b) 1%, and (c) 1.5 %.

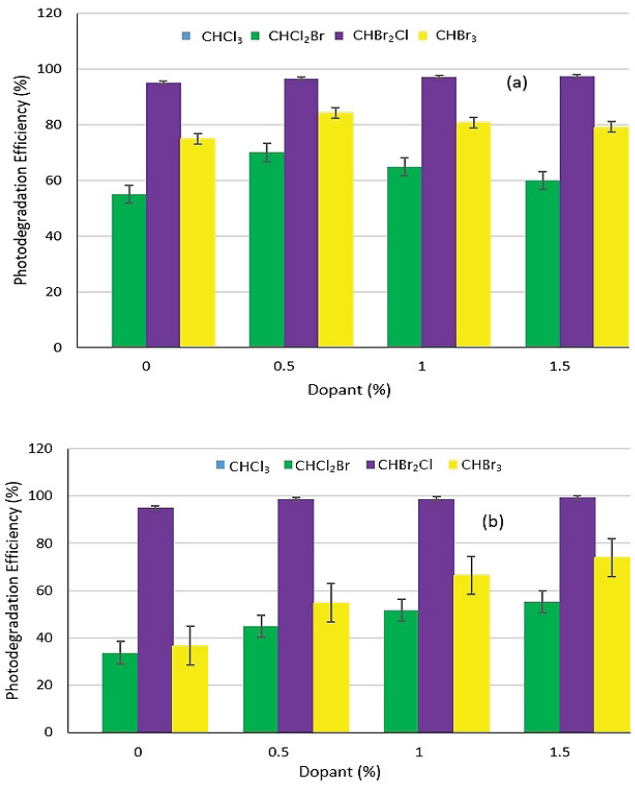

Fig. 6. Effect of dopant weight percentage on photocatalytic efficiency of THMs using Zr:ZnO NPs under (a) UV and (b) sunlight illumination.

of each sample was determined (56%, 57%, 58% and 65% for sunlight and 40%, 45%, 47%, and 52% for UV light illumination, respectively (Fig. 7). With increasing time, the removal rate decreases due to the increase in the amount of electron excitation and thus increases the electron-hole pair produced, and as the irradiation time increases, more electrons and more hydroxyl radicals are produced, which cause oxidation and increased degradation of trihalomethanes with increasing time [26,47].

3.2.3. Effect of Zr:ZnO NPs dosage

In order to determine the effect of nanoparticle dosage on the photodegradation efficiency, samples with a concentration of 40 ppb were prepared by adding different nanoparticle dosage (0.5, 1.0, 1.5, and 2 g/L) and each sample was exposed to light source for 120 min. After the desired time, the removal efficiency of each sample was determined (51%, 56%, 60%, and 67% for sunlight and 46%, 48%, 53%, and 51% for UV light illumination, respectively). As Fig. 8 shows, in the samples irradiated with sunlight, with increasing the dosage of nanoparticles, the removal efficiency increased, which can be attributed to the increase in the production of electron-hole pairs and consequently the oxidizing radicals produced due to increasing the concentration of nanoparticles [48]. In UV-irradiated samples, increasing the dosage to an optimal level can increase the rate of degradation; by increasing the dosage of nanoparticles more than the optimum amount, the removal efficiency decreases slightly, which can be attributed to the turbidity created by the nanoparticle, reducing the penetration of UV

light and the competition for reaction with hydroxyl radicals at high concentrations [49].

Finally, optimum conditions for the photodegradation of trihalomethanes under UV irradiation was contact time of 120 min and 1.5 g/L 1% Zr:ZnO NPs; under such condition, the removal percentage of bromoform, bromomethane chloride, dichlorobromomethane, and total trihalomethane was 79.25%, 96.5%, 65%, and 52%, respectively. Whereas, it was found that the optimum condition under sunlight illumination was contact time of 120 min and 2.0 g/L 1.5% Zr:ZnO NPs; under such condition, the removal percentage of chloroform, bromoform, bromomethane chloride,

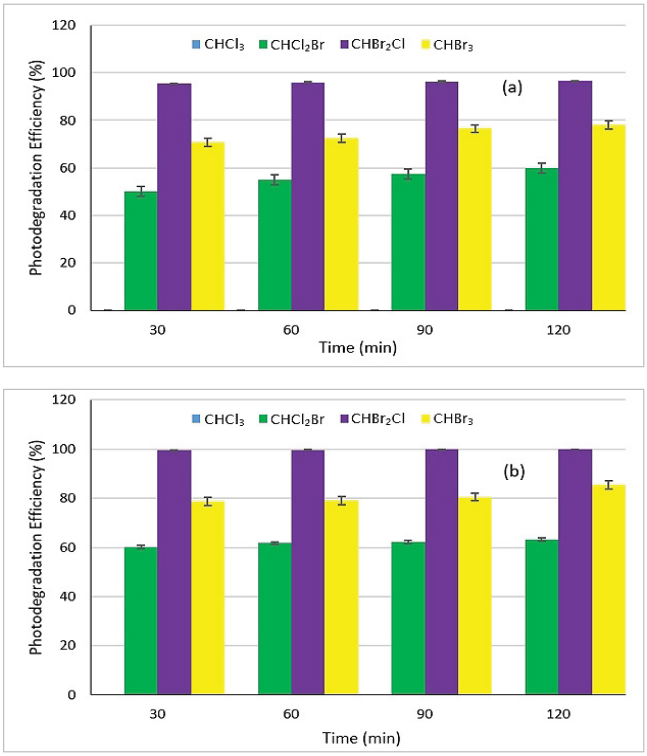

Fig. 7. Effect of contact time on photocatalytic efficiency of THMs using Zr:ZnO NPs under (a) UV and (b) sunlight illumination.

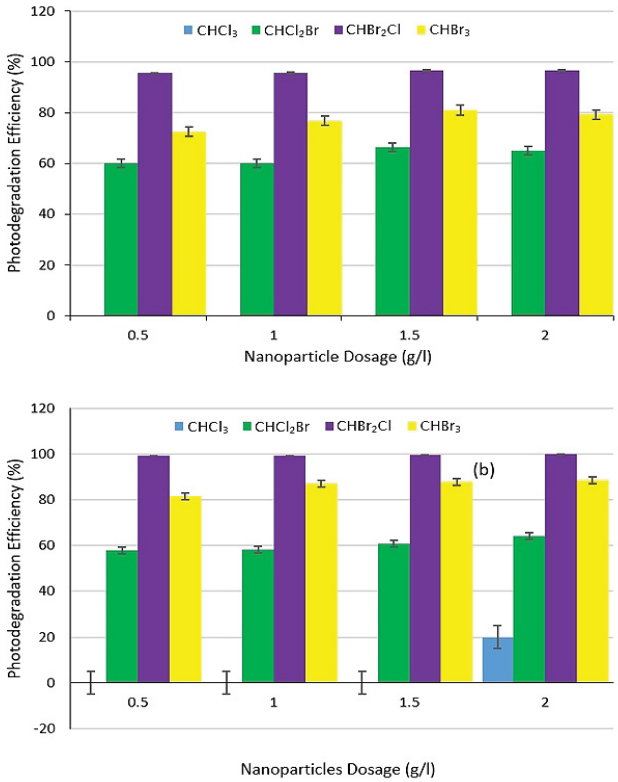

Fig. 8. Effect of Zr:ZnO NPs dosage on photocatalytic efficiency of THMs under (a) UV and (b) sunlight illumination.

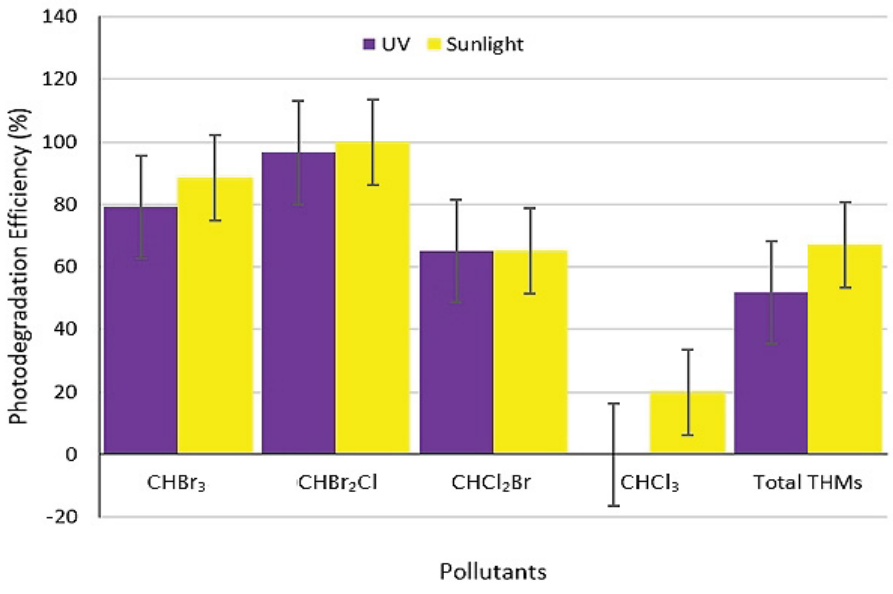

Fig. 9. Photodegradation efficiency of THMs using Zr:ZnO NPs under optimal conditions.

dichlorobromomethane, and total trihalomethane was 20%, 88.5%, 99.75%, 65%, and 67%, respectively (Fig. 9).

4. Conclusion

In this research, zirconium doped zinc oxide nanoparticles (Zr:ZnO NPs) were prepared by hydrothermal method. The structure, morphology and optical properties of the synthesized zinc oxide nanoparticles were investigated by different techniques. It was found that the dopant percentage does not change the particles' structure but it could control the morphology. Moreover, the application of surface modifier could help in controlling particle size distribution. FTIR showed certain functional group on the particles synthesized, as the effect of n-butylamine added as surface modifier. Chloroform could be slightly degraded under sunlight illumination but UV had no effect on its photodegradation. The dopant weight percentage play a crucial role on the photodegradation efficiency depending on the light source; in our study, 1.0% and 1.5% showed the highest photodegradation efficiency of THMs under UV and sunlight illumination, respectively. One of the limitations of this work was studying on only one concentration of THMs. It is suggested to study this parameter in depth as the condition of each treatment plant and water quality differs.

Acknowledgement

The authors would like to thank Kurdistan University of Medical Sciences for supports provided under Grant Number IR.MUK.REC.1399.088. This research was also supported by Basic Science Research Program through the National Research Foundation of Korea (NRF) funded by the Ministry of Education (NRF-2019R1I1A3A01062424). This study was also partially supported by International Affairs Division of Khon Kaen University (International Visiting Scholar, 2019 for Assoc. Prof. Behzad Shahmoradi).

References

[1] A. Yazdanbakhsh, M. Leili, M. Rezazadeh Azari, M. Masoudinejad, M. Majlesi, Chloroform concentration in drinking water of Tehran, 2009, J. Mazandaran Univ. Med. Sci., 24 (2014) 102–113.
[2] A. Ahamad, S. Madhav, A.K. Singh, A. Kumar, P. Singh, Types of Water Pollutants: Conventional and Emerging, D. Pooja, P. Kumar, P. Singh, S. Patil, Eds., Sensors in Water Pollutants Monitoring: Role of Material, Advanced Functional Materials and Sensors, Springer, Singapore, 2020, pp. 21–41.
[3] S. Anand, B. Philip, H. Mehendale, Chlorination By-products, 2014.
[4] S. Tsitsifli, V. Kanakoudis, Disinfection impacts to drinking water safety—a review, Proceedings, 2 (2018) 603, doi: 10.3390/proceedings2110603.
[5] A. Kwarciak-Kozłowska, Chapter 1 – Methods Used for the Removal of Disinfection By-products from Water, M.N. Vara Prasad, Ed., Disinfection By-products in Drinking Water, Elsevier, 2020, pp. 1–21.
[6] A. Nasiri, N. Jaafarzadeh, T. Tabatabaie, F. Amiri, A. Pazira, Trihalomethane formation potential in rural drinking water: a case study project of Seven Villages - Marvdasht Fars, J. Environ. Treat. Tech., 8 (2020) 107–111.
[7] M. Saidan, K. Rawajfeh, M. Fayyad, Investigation of factors affecting THMs formation in drinking water, Am. J. Environ. Eng., 3 (2013) 207–212.
[8] K.P. Singh, P. Rai, P. Pandey, S. Sinha, Modeling and optimization of trihalomethanes formation potential of surface water (a drinking water source) using Box–Behnken design, Environ. Sci. Pollut. Res., 19 (2012) 113–127.
[9] N.I. Hasan, H.F. Makki, Disinfection by-product removal by activated carbon-using batch mode, IOP Conf. Ser.: Earth Environ. Sci., 790 (2021) 012035.
[10] H. MacKeown, J.A. Gyamfi, M. Delaporte, K.V.K.M. Schoutteten, L. Verdickt, B. Ouddane, J. Criquet, Removal of disinfection by-product precursors by ion exchange resins, J. Environ. Chem. Eng., 9 (2021) 104602, doi: 10.1016/j.jece.2020.104602.
[11] P. Maćczak, H. Kaczmarek, M. Ziegler-Borowska, Recent achievements in polymer bio-based flocculants for water treatment, Materials (Basel), 13 (2020) 3951, doi: 10.3390/ma13183951.
[12] M.C. Mbaeze, V. Agbazue, N. Orjioke, Comparative assessment of performance of aluminium sulphate (alum) and ferrous sulphate as coagulants in water treatment, Mod. Chem., 5 (2017) 1–14.
[13] S.M. Bachand, T.E.C. Kraus, D. Stern, Y.L. Liang, W.R. Horwath, P.A.M. Bachand, Aluminum- and iron-based coagulation for in-situ removal of dissolved organic carbon, disinfection by-products, mercury and other constituents from agricultural drain water, Ecol. Eng., 134 (2019) 26–38.
[14] D. Ghernaout, N. Elboughdiri, Disinfection by-products: presence and elimination in drinking water, Open Access Library J., 7 (2020) 1–27.
[15] Q. Lin, F. Dong, Y. Miao, C. Li, W. Fei, Removal of disinfection by-products and their precursors during drinking water treatment processes, Water Environ. Res., 92 (2020) 698–705.
[16] K. Qi, B. Cheng, J. Yu, W. Ho, Review on the improvement of the photocatalytic and antibacterial activities of ZnO, J. Alloys Compd., 727 (2017) 792–820.
[17] M. Adeel, M. Saeed, I. Khan, M. Muneer, N. Akram, Synthesis and characterization of Co–ZnO and evaluation of its photocatalytic activity for photodegradation of methyl orange, ACS Omega, 6 (2021) 1426–1435.
[18] R. Ameta, S.C. Ameta, Photocatalysis: Principles and Applications, CRC Press, 2016.
[19] O. Długosz, K. Szostak, M. Banach, Photocatalytic properties of zirconium oxide–zinc oxide nanoparticles synthesised using microwave irradiation, Appl. Nanosci., 10 (2020) 941–954.
[20] C.B. Ong, L.Y. Ng, A.W. Mohammad, A review of ZnO nanoparticles as solar photocatalysts: synthesis, mechanisms and applications, Renewable Sustainable Energy Rev., 81 (2018) 536–551.
[21] X. Chen, Z. Wu, D. Liu, Z. Gao, Preparation of ZnO photocatalyst for the efficient and rapid photocatalytic degradation of azo dyes, Nanoscale Res. Lett., 12 (2017) 1–10.
[22] B. Shahmoradi, K. Namratha, K. Byrappa, K. Soga, S. Ananda, R. Somashekar, Enhancement of the photocatalytic activity of modified ZnO nanoparticles with manganese additive, Res. Chem. Intermed., 37 (2011) 329–340.
[23] N. Clament Sagaya Selvam, J.J. Vijaya, L.J. Kennedy, Effects of morphology and Zr doping on structural, optical, and photocatalytic properties of ZnO nanostructures, Ind. Eng. Chem. Res., 51 (2012) 16333–16345.
[24] A.T. Oluwabi, A.O. Juma, I.O. Acik, A. Mere, M. Krunks, Effect of Zr doping on the structural and electrical properties of spray deposited TiO_2 thin films, Proc. Estonian Acad. Sci., 67 (2018) 147–157.
[25] G. Kale, S. Arbuj, U. Kawade, S. Kadam, L. Nikam, B. Kale, Paper templated synthesis of nanostructured Cu–ZnO and its enhanced photocatalytic activity under sunlight, J. Mater. Sci. - Mater. Electron., 30 (2019) 7031–7042.
[26] D.D. Zhang, R.L. Qiu, S.Z. Wang, Visible light induced photocatalytic degradation of Br-trihalomethanes over polymer-modified TiO_2, Adv. Mater. Res., 726–731 (2013) 2372–2375.
[27] A.R. Abhijith, A.K. Srivastava, A. Srivastava, Synthesis and characterization of magnesium doped ZnO using chemical route, J. Phys. Conf. Ser., 1531 (2020) 012005.
[28] T. Chitradevi, A.J. Lenus, N.V. Jaya, Structure, morphology and luminescence properties of sol-gel method synthesized pure

and Ag-doped ZnO nanoparticles, Mater. Res. Express, 7 (2019) 015011.
[29] P. Raizada, A. Sudhaik, P. Singh, Photocatalytic water decontamination using graphene and ZnO coupled photocatalysts: a review, Mater. Sci. Energy Technol., 2 (2019) 509–525.
[30] A.C. Mohan, B. Renjanadevi, Preparation of zinc oxide nanoparticles and its characterization using scanning electron microscopy (SEM) and X-ray diffraction (XRD), Procedia Technol., 24 (2016) 761–766.
[31] M.C. Uribe-López, M.C. Hidalgo-López, R. López-González, D.M. Frías-Márquezc, G. Núñez-Nogueiraa, D. Hernández-Castilloc, M.A. Alvarez-Lemus, Photocatalytic activity of ZnO nanoparticles and the role of the synthesis method on their physical and chemical properties, J. Photochem. Photobiol., A, 404 (2021) 112866, doi: 10.1016/j.jphotochem.2020.112866.
[32] B.J. Warner, S.C. Cheng, J.M. Fenke, C.S. Friedman, S. Mitrosky, S.D. Snyder, C.R. McMilian, EPA Method Study 23B, Method 501.2, Trihalomethanes by Liquid/Liquid Extraction, Environmental Monitoring and Support Laboratory, Cincinnati OH 45268, 1986.
[33] A. Precious Ayanwale, S.N.Y. Reyes-López, ZrO_2–ZnO nanoparticles as antibacterial agents, ACS Omega, 4 (2019) 19216–19224.
[34] R. Rajendran, A. Mani, Photocatalytic, antibacterial and anticancer activity of silver-doped zinc oxide nanoparticles, J. Saudi Chem. Soc., 24 (2020) 1010–1024.
[35] N.M. Shamhari, B. Siong-Wee, S.F. Chin, K.Y. Kok, Synthesis and characterization of zinc oxide nanoparticles with small particle size distribution, Acta Chim. Slov., 65 (2018) 578–585.
[36] F.K. Konan, B. Hartiti, A. Batan, B. Aka, X-ray diffraction, XPS, and Raman spectroscopy of coated ZnO:Al (1–7 at%) nanoparticles, e-J. Surf. Sci. Nanotechnol., 17 (2019) 163–168.
[37] T. Suwannaruang, J.P. Hildebrand, D.H. Taffa, M. Wark, K. Kamonsuangkasem, P. Chirawatkul, K. Wantala, Visible light-induced degradation of antibiotic ciprofloxacin over Fe–N–TiO_2 mesoporous photocatalyst with anatase/rutile/brookite nanocrystal mixture, J. Photochem. Photobiol., A, 391 (2020) 112371, doi: 10.1016/j.jphotochem.2020.112371.
[38] S. Han, D. Zhao, T. Otroshchenko, H. Lund, U. Bentrup, V.A. Kondratenko, N. Rockstroh, S. Bartling, D.E. Doronkin, J.D. Grunwaldt, U. Rodemerck, D. Linke, M. Gao, G. Jiang, E.V. Kondratenko, Elucidating the nature of active sites and fundamentals for their creation in Zn-containing ZrO_2–based catalysts for nonoxidative propane dehydrogenation, ACS Catal., 10 (2020) 8933–8949.
[39] M. Ismail, M.K. Rahmani, S.A. Khan, J. Choi, F. Hussain, Z. Batool, A.M. Rana, J. Lee, H. Cho, S. Kim, Effects of Gibbs free energy difference and oxygen vacancies distribution in a bilayer ZnO/ZrO_2 structure for applications to bipolar resistive switching, Appl. Surf. Sci., 498 (2019) 143833, doi: 10.1016/j.apsusc.2019.143833.
[40] J. Winiarski, W. Tylus, K. Winiarska, I. Szczygieł, B. Szczygieł, XPS and FT-IR characterization of selected synthetic corrosion products of zinc expected in neutral environment containing chloride ions, J. Spectrosc., 2018 (2018) 2079278, doi: 10.1155/2018/2079278.
[41] S. Alamdari, M. Sasani Ghamsari, C. Lee, W. Han, H.-H. Park, M. Jafar Tafreshi, H. Afarideh, M.H. Majles Ara, Preparation and characterization of zinc oxide nanoparticles using leaf extract of *Sambucus ebulus*, Appl. Sci., 10 (2020) 3620, doi: 10.3390/app10103620.
[42] O.V. Ovchinnikov, A.V. Evtukhova, T.S. Kondratenko, M.S. Smirnov, V.Y. Khokhlov, O.V. Erina, Manifestation of intermolecular interactions in FTIR spectra of methylene blue molecules, Vib. Spectrosc., 86 (2016) 181–189.
[43] S. Bhattacharjee, DLS and zeta potential–what they are and what they are not?, J. Control Release, 235 (2016) 337–351.
[44] Z. Vasiljevic, M.P. Dojcinovic, J.D. Vujancevic, I. Jankovic-Castvan, M. Ognjanovic, N.B. Tadic, S. Stojadinovic, G.O. Brankovic, M.V. Nikolic, Photocatalytic degradation of methylene blue under natural sunlight using iron titanate nanoparticles prepared by a modified sol–gel method, R. Soc. Open Sci., 7 (2020) 200708, doi: 10.1098/rsos.200708.
[45] M.M. Kondo, W.F. Jardim, Photodegradation of chloroform and urea using Ag-loaded titanium dioxide as catalyst, Water Res., 25 (1991) 823–827.
[46] X. Chang, X. Yao, N. Ding, X. Yin, Q. Zheng, S. Lu, D. Shuai, Y. Sun, Photocatalytic degradation of trihalomethanes and haloacetonitriles on graphitic carbon nitride under visible light irradiation, Sci. Total Environ., 682 (2019) 200–207.
[47] S. Yakout, Removal of trihalomethanes from aqueous solution through adsorption and photodegradation, Adsorpt. Sci. Technol., 28 (2010) 601–610.
[48] C. Kormann, D.W. Bahnemann, M.R. Hoffmann, Photolysis of chloroform and other organic molecules in aqueous titanium dioxide suspensions, Environ. Sci. Technol., 25 (1991) 494–500.
[49] K.M. Lee, C.W. Lai, K.S. Ngai, J.C. Juan, Recent developments of zinc oxide based photocatalyst in water treatment technology: a review, Water Res., 88 (2016) 428–448.